A Robust Field Orientation Control Method for Induction Motor Drives

Peng Zeng, *Student Member, IEEE*, Yao Sun, *Member, IEEE*, Hanbing Dan, *Senior Member, IEEE*, Feng Zhou, *Member, IEEE*, Mei Su, *Member, IEEE*, and Patrick Wheeler, *Fellow, IEEE*

***Abstract*—The performance of the induction motor (IM) control system under the conventional rotor-flux-oriented scheme may greatly deteriorate in the presence of parameter mismatch. To address this problem, first, the motor parameters sensitivity of two different field orientation methods is analyzed. Then, a modified field orientation method, which combines the advantages of the two different field orientation methods, is presented. Compared with the conventional scheme, the proposed IM control scheme guarantees the robustness of the system against leakage inductance mismatch across the full load range, leading to static and dynamic high-speed performance improvement. Finally, the effectiveness of the proposed method is verified by simulations and experiments.**

***Index Terms*—Field orientation method, induction motor (IM) drive, parametric uncertainties, rotor-flux-oriented (RFO).**

NOMENCLATURE

Superscript ref	Reference value.
Superscript ˜	Error value.
Superscript ˆ	Estimated value.
Superscript -	Steady-state value.
$\mathbf{u}_s$	$= u_{sd} + ju_{sq}$. Synchronous-frame voltage vector.
$\mathbf{i}_s$	$= i_{sd} + ji_{sq}$. Synchronous-frame current vector.
$\boldsymbol{\psi}_s$	$= \psi_{sd} + j\psi_{sq}$. Synchronous-frame stator flux vector.
$\boldsymbol{\psi}_r$	$= \psi_{rd} + j\psi_{rq}$. Synchronous-frame rotor flux vector.
L_r	Rotor inductance.
L_m	Mutual inductance.
L_s	Stator inductance.
L_σ	$= L_r - {L_m^2}/{L_r}$. Leakage inductance.
R_s	Stator resistance.
R_r	Rotor resistance.
T_r	$= {L_r}/{R_r}$. Rotor time constant.
$\omega_1, \omega_r, \omega_s$	Synchronous angular speed, rotor angular speed, slip angular speed.
n_p	The number of pole pairs.
θ	Rotor flux phase angle.

Manuscript received 28 November 2023; revised 30 January 2024 and 30 March 2024; accepted 4 May 2024. Date of publication 13 May 2024; date of current version 20 June 2024. This work was supported by the National Natural Science Foundation of China under Grant 62125308, Grant 52337008, Grant 52277071, and Grant 52377168. Recommended for publication by Associate Editor D.-C. Lee. *(Corresponding authors: Yao Sun; Hanbing Dan.)*

Peng Zeng, Yao Sun, Hanbing Dan, and Mei Su are with the School of Automation, Central South University, Changsha 410083, China, and also with the Hunan Provincial Key Laboratory of Power Electronics Equipment and Grid, Changsha 410083, China (e-mail: pengzengcsu@csu.edu.cn; yaosun@mail.csu.edu.cn; hanbingdan@csu.edu.cn; sumeicsu@csu.edu.cn).

Feng Zhou is with the College of Electronic Information and Electrical Engineering, Changsha University, Changsha 410082, China (e-mail: zhoufeng@ccsu.edu.cn).

Patrick Wheeler is with the School of Electrical and Electronic Engineering, University of Nottingham, NG7 2RD Nottingham, U.K. (e-mail: Pat.Wheeler@nottingham.ac.uk).

Color versions of one or more figures in this article are available at https://doi.org/10.1109/TPEL.2024.3398684.

Digital Object Identifier 10.1109/TPEL.2024.3398684

I. INTRODUCTION

THE rotor-flux-oriented (RFO)-based induction motor (IM) drives with speed sensors are widely adopted in various electric vehicles due to their faster dynamic response, high reliability, and excellent performance [1], [2], [3]. The accuracy of the rotor flux angle is crucial for achieving RFO control. To obtain the rotor flux angle, a flux observer is commonly employed. There are two classic types of flux observers: voltage model [4], [5] and current model [4]. The voltage model exhibits excellent performance in the high-speed region because it is highly robust to the detuning of R_r and L_m. However, it has a high parameter sensitivity to L_σ at high speed [6]. On the contrary, the current model shows better performance at low speed. However, both flux observers mentioned previously rely on the accuracy of motor parameters. The motor parameter mismatch will lead to inaccurate field orientation, which degrades the control performance of the RFO-based IM drive systems.

To improve the performance of the RFO-based IM drive systems, there have been various approaches aiming at improving the accuracy of field orientation under parameter mismatch. These methods can be categorized into two types: parameter identification and robust flux observer design. In [7], [8], [9], [10], and[11], the approaches based on the model reference adaptive system (MRAS) are studied to identify parameters. The MRAS can be divided into q-axis rotor-flux-based [7], d-axis stator-voltage-based [8], [9], and reactive-power-based methods [10], [11]. These methods are built upon the model of IM, so their accuracy largely depends on the precision of the reference model. In [10] and [11], the rotor time constant was identified by the reactive power equation, which is independent of stator resistance. However, the method depends on the accuracy of leakage inductance. Unfortunately, the leakage inductance varies with the magnetic saturation of the leakage flux in the rotor core. Therefore, the robustness of the MRAS is

decreased in this condition. The schemes based on the extended Kalman filter (EKF) are described in [12] and [13]. Model uncertainty and nonlinearity inherent in IMs are well adapted to the stochastic nature of the EKF [13]. However, the EKF is computationally intensive. In [14] and [15], methods based on fuzzy logic and backstepping approach are proposed to estimate rotor resistance, respectively, which improves the robustness of the control system against the rotor resistance mismatch.

Another class of scheme is to improve the accuracy of field orientation by designing robust flux observers. Adaptive full-order state observers have been studied in [16], [17], [18], [19], and [20]. In [18], a method is proposed to compute the gains of IM flux observers and reduce observer sensitivity to rotor resistance uncertainty. In [19], an adaptive observer for online estimation of rotor and stator resistances is considered for IMs, while only one phase current is measured. In [20], an improved "phase-shift"-based compensation method is proposed to improve the accuracy and stability of the stator resistance estimator under different speeds and load torque conditions. The sliding mode observer has also been widely used because it has strong robustness to parametric uncertainties [21], [22], [23]. In [21], a sliding-mode observer is proposed due to its disturbances rejection, and strong robustness to parameter deviations. However, the discontinuous control laws bring unnecessary chatting to the system, which deteriorates the performance of the system. In [24], [25], [26], [27], [28], and [29], some approaches combining current and voltage models are proposed to improve the accuracy of field orientation. The Gopinath observers in [24], [25], and [26], reduced-order observers in [27] and [28], and full-order observers in [29] all adopt voltage model in the high-speed region. However, the voltage model has a high sensitivity to leakage inductance mismatch under large load conditions [6], [26], and these studies do not propose any specific methods for solving the issue. In addition, if leakage inductance is not accurately reflected in the estimation of the rotor flux, the torque of IM reveals an oscillatory response. In the extreme case, overcurrent fault and out-of-control phenomenon may occur [30], [31]. In [30], an overestimated leakage inductance is used to address the out-of-control problem. However, the problem of large field orientation errors caused by leakage inductance mismatch has not been solved. In summary, the problem that voltage model has a high sensitivity to leakage inductance mismatch under high speed and large load conditions has not yet been solved.

Therefore, this article aims to solve the problem that the voltage model-based drive system is sensitive to leakage inductance mismatch under high speed and large load conditions. The contribution of this article can be summarized as follows.

1) The influences of parameter mismatch on field orientation errors under different field orientation methods are analyzed, which provides insight into ideas of improving field orientation accuracy.
2) A robust field orientation scheme is proposed, which improves the robustness of the voltage model-based IM drives to leakage inductance mismatch at high speed and large load conditions, leading to a better speed response and an improvement in the antidisturbance ability of the IM.

The rest of this article is organized as follows. In Section II, the mathematical model of the IM is introduced. Section III compares the performance of two field orientation methods under parameter mismatch. The proposed field orientation method is presented in Section IV. Simulation and experimental results are presented in Sections V and VI, respectively. Finally, Section VII concludes this article.

II. Mathematical Model of the IM

The electromagnetic dynamic model of the IM in the synchronous *d–q* frame is described as follows:

$$\begin{cases} \frac{d\psi_{rd}}{dt} + \frac{1}{T_r}\psi_{rd} = (\omega_1 - \omega_r)\psi_{rq} + \frac{L_m}{T_r} i_{sd} \\ \frac{d\psi_{rq}}{dt} + \frac{1}{T_r}\psi_{rq} = -(\omega_1 - \omega_r)\psi_{rd} + \frac{L_m}{T_r} i_{sq} \end{cases} \tag{1}$$

$$\begin{cases} L_\sigma \frac{di_{sd}}{dt} = -Ri_{sd} + \omega_1 L_\sigma i_{sq} + \frac{L_m}{L_r T_r}\psi_{rd} \\ \qquad + \frac{L_m}{L_r}\omega_r \psi_{rq} + u_{sd} \\ L_\sigma \frac{di_{sq}}{dt} = -Ri_{sq} - \omega_1 L_\sigma i_{sd} + \frac{L_m}{L_r T_r}\psi_{rq} \\ \qquad - \frac{L_m}{L_r}\omega_r \psi_{rd} + u_{sq} \end{cases} \tag{2}$$

where $R = (R_s + \frac{L_m^2}{L_r^2} R_r)$.

The electromagnetic torque of the IM is expressed as

$$T_e = \frac{3}{2}\frac{L_m n_p}{L_r}\left(\psi_{rd} i_{sq} - \psi_{rq} i_{sd}\right). \tag{3}$$

Torque control is very critical for high-performance motor control. In the RFO control scheme, the electromagnetic torque and flux of IM can be independently controlled like a separately excited dc motor [32]. However, the precondition is that there is no field orientation error. Therefore, improving the field orientation accuracy is very essential in practice.

III. Flux Estimation Error Analysis

A. Influence of Parameter Mismatch on the Estimated Rotor Flux

The voltage equation in the synchronous *d-q* frame is represented as

$$\begin{cases} \frac{d\boldsymbol{\psi}_s}{dt} + j\omega_1 \boldsymbol{\psi}_\mathbf{s} = \mathbf{u_s} - R_s \mathbf{i_s} \\ \boldsymbol{\psi}_r = \frac{L_r}{L_m}\boldsymbol{\psi}_s - \frac{L_r}{L_m} L_\sigma \mathbf{i}_s. \end{cases} \tag{4}$$

Then, according to (4), the estimated rotor flux equations based on the voltage model are expressed as

$$\begin{cases} \frac{d\hat{\boldsymbol{\psi}}_s}{dt} + j\omega_1 \hat{\boldsymbol{\psi}}_\mathbf{s} = \mathbf{u_s} - \hat{R}_s \mathbf{i_s} \\ \hat{\boldsymbol{\psi}}_r = \frac{\hat{L}_r}{\hat{L}_m}\hat{\boldsymbol{\psi}}_s - \frac{\hat{L}_r}{\hat{L}_m}\hat{L}_\sigma \mathbf{i}_s. \end{cases} \tag{5}$$

Combining (4) with (5), the actual rotor flux and the estimated rotor flux in steady state are simply expressed as

$$\begin{cases} \bar{\boldsymbol{\psi}}_r = k_1 \bar{\mathbf{u}}_\mathbf{s} + k_2 \bar{\mathbf{i}}_s \\ \bar{\hat{\boldsymbol{\psi}}}_r = \hat{k}_1 \bar{\mathbf{u}}_\mathbf{s} + \hat{k}_2 \bar{\mathbf{i}}_s \end{cases} \tag{6}$$

where $k_1 = L_r/(L_m j\omega_1), k_2 = -(R_s/(j\omega_1) + L_\sigma)L_r/L_m$, and $\hat{k}_1 = \hat{L}_r/(\hat{L}_m j\omega_1), \hat{k}_2 = -(\hat{R}_s/(j\omega_1) + \hat{L}_\sigma)\hat{L}_r/\hat{L}_m$.

According to (6), the following relationship is obtained:

$$\bar{\boldsymbol{\psi}}_{\boldsymbol{r}} = \frac{k_1}{\hat{k}_1}\bar{\hat{\boldsymbol{\psi}}}_{\boldsymbol{r}} + \left(k_2 - \frac{k_1\hat{k}_2}{\hat{k}_1}\right)\bar{\mathbf{i}}_s. \tag{7}$$

According to (7), the following relationship in steady state is obtained (assuming $L_s = L_r$ [34]):

$$\begin{cases} \bar{\psi}_{rd} = \dfrac{\left(1+\frac{1}{2}n\right)\left(1-\tilde{L}\right)}{1-\tilde{L}+\frac{1}{2}n-\frac{1}{2}\tilde{n}}\bar{\hat{\psi}}_{rd} + \left(1+\frac{1}{2}n\right)L_m\bar{i}_{sd}\left(-\tilde{m}k-\tilde{n}\right) \\ \bar{\psi}_{rq} = \dfrac{\left(1+\frac{1}{2}n\right)\left(1-\tilde{L}\right)}{1-\tilde{L}+\frac{1}{2}n-\frac{1}{2}\tilde{n}}\bar{\hat{\psi}}_{rq} + \left(1+\frac{1}{2}n\right)L_m\bar{i}_{sd}\left(\tilde{m}-k\tilde{n}\right) \end{cases} \tag{8}$$

where $\tilde{n} = \frac{\tilde{L}_\sigma}{L_m}$, $\tilde{m} = \frac{\tilde{R}_s}{\omega_1 L_m}$, $\tilde{L} = \frac{\tilde{L}_m}{L_m}$, $\tilde{R}_s = R_s - \hat{R}_s$, $\tilde{L}_m = L_m - \hat{L}_m$, $\tilde{L}_\sigma = L_\sigma - \hat{L}_\sigma$, $k = \frac{\bar{i}_{sq}}{\bar{i}_{sd}}$, and $n = \frac{L_\sigma}{L_m}$.

The following relationship can be derived by the linearization of (8) at the point where the parameter errors are zero:

$$\bar{\psi}_{rq} = \left(1 + \frac{\frac{1}{2}\tilde{n} - \frac{1}{2}n\tilde{L}}{1+\frac{1}{2}n}\right)\bar{\hat{\psi}}_{rq} + \left(1+\frac{1}{2}n\right)L_m\bar{i}_{sd}\left(\tilde{m}-k\tilde{n}\right) \tag{9a}$$

$$\bar{\psi}_{rd} = \left(1 + \frac{\frac{1}{2}\tilde{n} - \frac{1}{2}n\tilde{L}}{1+\frac{1}{2}n}\right)\bar{\hat{\psi}}_{rd} + \left(1+\frac{1}{2}n\right)L_m\bar{i}_{sd}\left(-\tilde{m}k-\tilde{n}\right). \tag{9b}$$

Clearly, it is difficult to make $\bar{\psi}_{rq} = 0$ in the presence of parameter errors.

B. Field Orientation Methods

As the estimated rotor flux is not the actual one due to parametric uncertainties, there are two field orientation methods to achieve the RFO control. One is the conventional RFO method (Method A), where the d-axis of the synchronous rotating coordinate frame is aligned with the estimated rotor flux vector

$$\bar{\hat{\psi}}_{rq} = 0. \tag{10}$$

The other is the method B, which is proposed in this article. Under the field orientation angle of the method, the following equation is satisfied:

$$\bar{\hat{\psi}}_{rd} = \hat{L}_m\bar{i}_{sd}. \tag{11}$$

It can be found that method A and method B are equivalent when the parameters are accurate. However, they have different effects on the field orientation error when the parameters are inaccurate. To compare the sensitivity under the two field orientation schemes to motor parameter mismatch, the field orientation errors under the two methods with parameter mismatch are subsequently analyzed.

C. Field Orientation Angle Error Analysis Under Method A

In this subsection, the field orientation angle error under method A is calculated.

The spatial relationship between the estimated rotor flux and the actual rotor flux is shown in Fig. 1, where $\tilde{\theta}$ is the field orientation angle error. And $\tilde{\theta}$ is expressed as

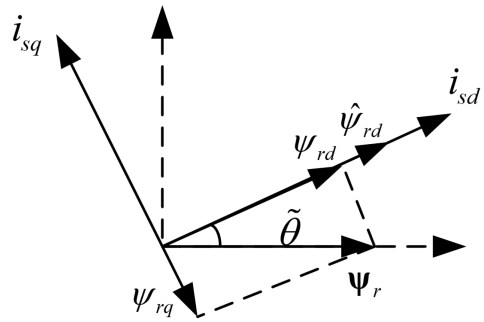

Fig. 1. Spatial relationship between the estimated and actual rotor flux.

$$\tilde{\theta} = -\tan^{-1}\frac{\bar{\psi}_{rq}}{\bar{\psi}_{rd}}. \tag{12}$$

By combining (9a) with (10), it is found that

$$\bar{\psi}_{rq} = \left(1+\frac{1}{2}n\right)L_m\bar{i}_{sd}\left(\tilde{m}-k\tilde{n}\right). \tag{13}$$

According to (1), the following steady-state relationship is obtained:

$$\bar{\psi}_{rd}^2 + \bar{\psi}_{rq}^2 - L_m\bar{i}_{sd}\bar{\psi}_{rd} - L_m\bar{i}_{sq}\bar{\psi}_{rq} = 0. \tag{14}$$

Usually, $\bar{\psi}_{rd} > 0$ and $|\bar{\psi}_{rd}| \gg |\bar{\psi}_{rq}|$, so according to (13) and (14), $\bar{\psi}_{rd}$ is given by

$$\bar{\psi}_{rd} = L_m\bar{i}_{sd}f_1(k) \tag{15}$$

where $f_1(k)$ can be found in the Appendix.

By combining (12) with (13) and (15), the field orientation angle error is expressed as

$$\tilde{\theta} = -\tan^{-1}\frac{\left(1+\frac{1}{2}n\right)\left(\tilde{m}-k\tilde{n}\right)}{f_1(k)}. \tag{16}$$

D. Field Orientation Angle Error Analysis Under Method B

In this subsection, the field orientation angle error under method B is calculated.

From (9b) and (11), $\bar{\psi}_{rd}$ is expressed as

$$\bar{\psi}_{rd} = L_m\bar{i}_{sd}f_2(k) \tag{17}$$

where $f_2(k)$ can be found in the Appendix.

Usually, $|\bar{\psi}_{rd}| \gg |\bar{\psi}_{rq}|$, so combining (14) and (17) yields

$$\bar{\psi}_{rq} = L_m\bar{i}_{sd}f_3(k) \tag{18}$$

where $f_3(k)$ is explained in the Appendix.

According to (12), (17), and (18), the field orientation angle error is expressed as

$$\tilde{\theta} = -\tan^{-1}\frac{f_3(k)}{f_2(k)}. \tag{19}$$

E. Parameters Sensitivity Comparison

According to (16) and (19), the field orientation errors under methods A and B with parameter mismatch are plotted in Figs. 2–4.

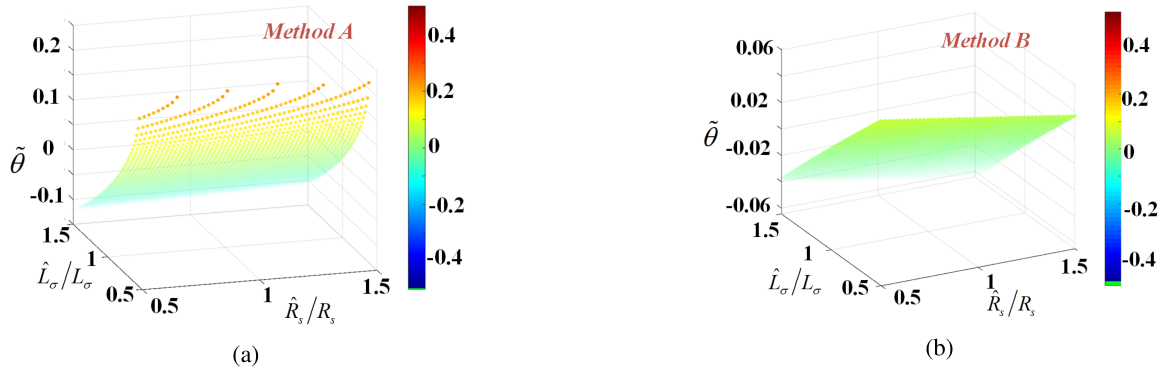

Fig. 2. Field orientation angle errors with variations in $\hat{R}_s$ and $\hat{L}_\sigma$ when $\omega_1 = 400$rad/s and $k = 2$. (a) Method A. (b) Method B.

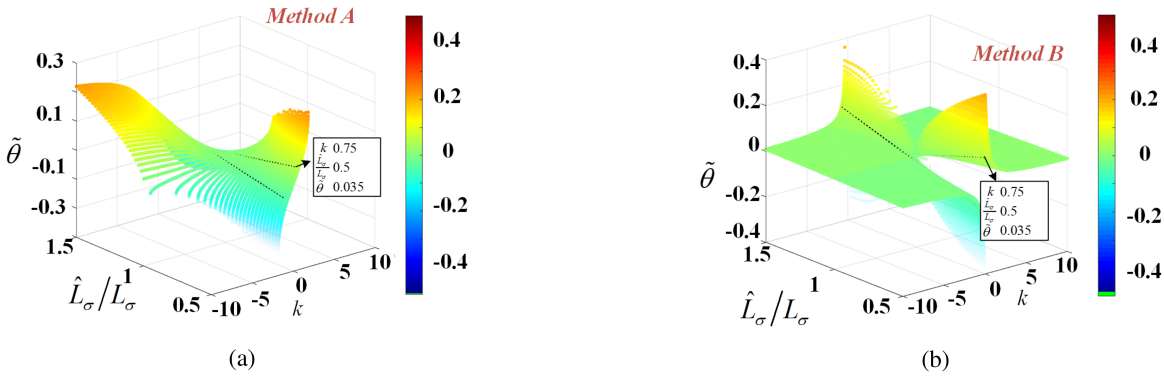

Fig. 3. Field orientation angle errors with variations in k and $\hat{L}_\sigma$ when $\omega_1 = 400$rad/s and $\hat{R}_s = 0.5R_s$. (a) Method A. (b) Method B.

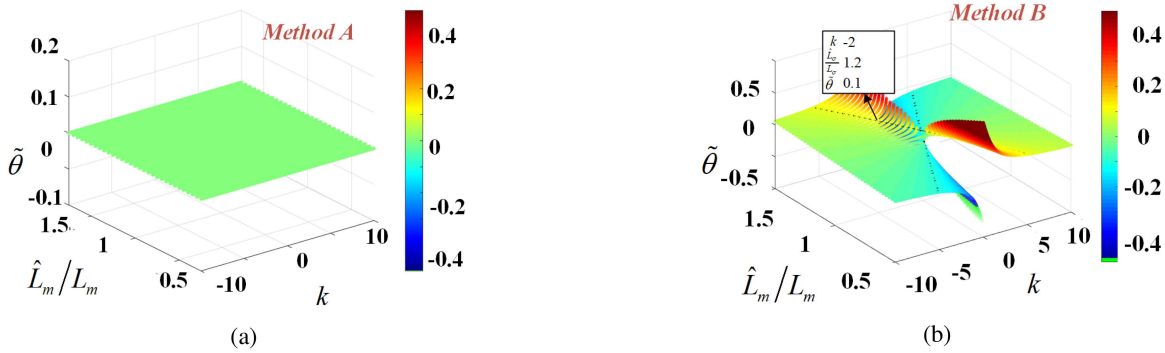

Fig. 4. Field orientation angle errors with variations in k and $\hat{L}_m$ when $\omega_1 = 400$rad/s. (a) Method A. (b) Method B.

Fig. 2 shows the field orientation errors under the two methods with leakage inductance and stator resistance mismatch when $k = 2$. As seen, method A is robust to stator resistance mismatch but very sensitive to leakage inductance mismatch. While method B is robust to both stator resistance and leakage inductance mismatch.

Fig. 3 shows the field orientation errors under the two methods with leakage inductance mismatch and k variations. The intersection lines of the error curves under methods A and B are displayed with dashed lines. As seen, method A is more robust to leakage mismatch when $|k|$ is relatively small, while method B is more robust when $|k|$ is relatively large.

Fig. 4 shows the field orientation errors under the two methods with mutual inductance mismatch and k variations. The flux angle error curves under method B with $\tilde{\theta} = \pm 0.1$ rad ($\pm 5.7°$) are highlighted with the black dashed line. As seen, method A is robust to mutual inductance mismatch across the full load range, method B is more sensitive to the deviation of L_m when $|k|$ is small, but the sensitivity decreases when $|k|$ is large.

Based on the aforementioned analysis, leakage inductance and mutual inductance are the main parameters that affect the flux orientation accuracy of the two schemes. Because mutual inductance identification technology is mature and simple [34], mutual inductance online updating technology is adopted [35].

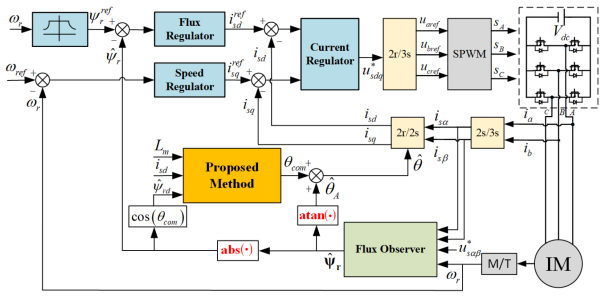

Fig. 5. Overall control block diagram of the proposed method.

Therefore, in the following analysis, the mutual inductance mismatch is assumed to be limited within a small range. Then, we could focus our attention on designing a control scheme, which is robust to variations of leakage inductance.

IV. Proposed Scheme

A. Proposed Robust Field Orientation Method

Based on the aforementioned analysis, the overall control block diagram of the proposed method is presented in Fig. 5. The proposed field orientation scheme combining methods A and B is expressed as

$$\hat{\theta} = \begin{cases} \hat{\theta}_A, & |k| \leqslant C \\ \hat{\theta}_B, & |k| > C \end{cases} \tag{20}$$

where $\hat{\theta}_A$ and $\hat{\theta}_B$ represent the field orientation angle under methods A and B, respectively, and C is a positive constant, which represents the switching point between the two methods.

The field orientation angle under method A can be calculated as

$$\hat{\theta}_A = \tan^{-1}\left(\frac{\mathrm{Im}\left(\hat{\boldsymbol{\psi}}_{\mathbf{r}}\right)}{\mathrm{Re}\left(\hat{\boldsymbol{\psi}}_{\mathbf{r}}\right)}\right) \tag{21}$$

where $\mathrm{Im}(\hat{\boldsymbol{\psi}}_{\mathbf{r}})$ and $\mathrm{Re}(\hat{\boldsymbol{\psi}}_{\mathbf{r}})$ represent the imaginary part and real part of $\hat{\boldsymbol{\psi}}_{\mathbf{r}}$, respectively.

However, the field orientation angle under method B cannot be obtained directly. In this study, a closed-loop controller is designed to obtain the field orientation angle, which is expressed as

$$\hat{\theta}_B = \hat{\theta}_A + \theta_{\mathrm{com}} \tag{22}$$

where θ_{com} represents the compensation angle, which is obtained by

$$\theta_{\mathrm{com}} = \left(k_p + \frac{k_i}{s}\right) y(s) \tag{23}$$

where $y(s) = \mathcal{L}\{y\}$, and $y = \hat{\psi}_{rd} - \hat{L}_m i_{sd}^{ref}$. And i_{sd}^{ref} represents the reference field current.

To achieve a smooth transition between the two methods, the output saturation of the proportional-integral (PI) controller (23) is designed as follows:

$$\theta_{\mathrm{com}}^{\max} = \begin{cases} 0, & |k| \leqslant C \\ (|k| - C)\,\Gamma, & |k| > C \end{cases} \tag{24}$$

where $\theta_{\mathrm{com}}^{\max}$ and $\theta_{\mathrm{com}}^{\min}$ represent the maximum and minimum allowed value of θ_{com}, respectively. Γ is a positive constant that adjusts $\theta_{\mathrm{com}}^{\max}$ and $\theta_{\mathrm{com}}^{\min}$. In addition, to avoid degradation of the controller performance caused by the saturation of the PI controller, the antisaturation method in [36] is adopted. Compared with method A, the proposed method needs an additional PI controller.

B. Stability Analysis

Assuming the bandwidth of (23) is much smaller than that of flux and current and the current controller is well designed, i.e., $i_{sd}^{\mathrm{ref}} = i_{sd}$. Then, according to (1), (9b), (12), and (14), the following relation can be obtained:

$$y = \omega_s k_m \tan\tilde{\theta} + d\left(\tilde{n}, \tilde{m}, \tilde{L}\right) \tag{25}$$

where ω_s represents slip angular speed, and ω_s, k_m, and d can be found in the Appendix. The angle error $\tilde{\theta}$ is expressed as

$$\tilde{\theta} = \hat{\theta}_B - \theta. \tag{26}$$

The following can be derived by the linearization of (26) at the point where the field orientation angle error is zero:

$$\Delta y = K\Delta\tilde{\theta} \tag{27}$$

where $K = \omega_s k_m$. And according to (22), (23), and (26), $\Delta\tilde{\theta}$ is expressed as

$$\Delta\tilde{\theta} = \Delta\hat{\theta}_B = \Delta\theta_{\mathrm{com}} = (k_p + \frac{k_i}{s})\Delta y(s). \tag{28}$$

By combining (27) and (28), the closed-loop characteristic equation is obtained

$$\Delta\tilde{\theta} = \left(k_p + \frac{k_i}{s}\right) K\Delta\tilde{\theta}. \tag{29}$$

From (29), the pole of the closed-loop system is expressed as

$$p = \frac{Kk_i}{1 - Kk_p}. \tag{30}$$

To ensure stability, k_p and k_i should be designed to make the pole less than zero. So, we have

$$\begin{cases} k_p \geq 0, k_i > 0, & \omega_s > 0 \\ k_p \leq 0, k_i < 0, & \omega_s < 0 \end{cases} \tag{31}$$

where ω_s represents slip angular speed, which is obtained by the method in [32].

C. Controller Parameters Selections

1) Selections for C and Γ: According to (22) and (24), the field orientation angle under the proposed scheme is expressed as

$$\hat{\theta} = \begin{cases} (1 - g_1)\,\theta_A + g_1\theta_B, & g_1 \leq 1 \\ \theta_B, & g_1 > 1 \end{cases} \tag{32}$$

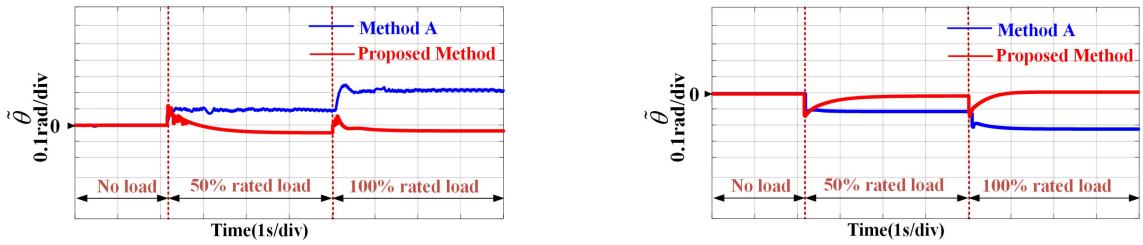

Fig. 6. Flux angle error comparison results for leakage inductance mismatch. (a) $\hat{L}_\sigma = 0.5L_\sigma$. (b) $\hat{L}_\sigma = 1.5L_\sigma$.

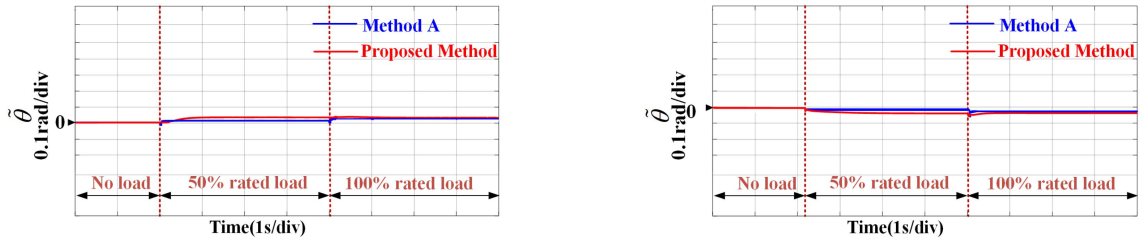

Fig. 7. Flux angle error comparison results for stator resistance mismatch. (a) $\hat{R}_s = 0.5R_s$. (b) $\hat{R}_s = 1.5R_s$.

where $g_1 = \theta_{\text{com}}^{\max}|\theta_B - \theta_A|$, which represents the gain coefficient. According to (32), the proposed scheme can be expressed as the sum of methods A and B, weighted by $1 - g_1$ and g_1, respectively.

According to Fig. 3, the field orientation error curves under methods A and B intersect at approximately $|k| = 1$. So, according to (24) and (32), the gain C is set to 1 to make method B work when $|k| > 1$. According to Fig. 4(b), with a 20% margin of mutual inductance errors, method B shows small field orientation errors (0.1 rad) when $k = 2$. Therefore, the gain Γ is set to 0.15 to make method B play a dominant role when $|k| \geq 2$.

2) Selections for k_p and k_i: The pole of the angle-compensated closed-loop system can be obtained from (30) and (31) (when approximating $|\frac{1}{2}\tilde{n}| \ll 1$, $\bar{\psi}_{\text{rd}} = \psi_r^{\text{ref}}$)

$$p = \frac{-|\omega_s| T_r \psi_r^{\text{ref}} |k_i|}{1 + |\omega_s| T_r \psi_r^{\text{ref}} |k_p|}. \tag{33}$$

First, the bandwidth of the angle-compensated closed-loop system should be significantly smaller than that of the flux loop. In addition, considering the speed drive performance, it should be larger than that of the speed loop. In the study, it should satisfy

$$2a_\omega < |p| \leq 0.1a_\psi \tag{34}$$

where a_ω and a_ψ are the bandwidth of the speed loop and flux loop, respectively. In the study, the gains k_p and k_i are designed as follows:

$$\begin{cases} k_p = \frac{k_i}{50} \\ \frac{2a_\omega}{k_s(1+2a_\omega 50)} < |k_i| \leq \frac{0.1a_\psi}{k_s(1+0.1a_\psi 50)} \end{cases} \tag{35}$$

where $k_s = \omega_s^{\text{rated}} T_r \psi_r^{\text{ref}}$, and ω_s^{rated} is the rated slip angular speed.

TABLE I
PARAMETERS OF THE IM

Quantity	Value	Quantity	Value
Rated power	0.68 kW	Stator resistance	0.0147 Ω
Rated voltage	14 V	Rotor resistance	0.013 Ω
Rated current	50 A	Stator/rotor inductance	1.57 mH
Rated frequency	70 Hz	Pole pairs	2
Rated torque	3 N.m	Sampling frequency	8 kHz

V. SIMULATION RESULTS

In this section, the effectiveness of the proposed control scheme is verified by simulations. The Gopinath observer in [25] is adopted as an example to verify the effectiveness of the proposed scheme. The motor parameters are listed in Table I. The gains of controllers are designed by the methods in [30], and these gains will be updated for all parameter mismatch cases. The base speed that enters the flux-weakening region is set to 925 r/min. All results are carried out in the flux-weakening region with a speed reference of 2000 r/min. The load torque is stepped through the sequence 50% and 100% rated load torque.

Fig. 6 shows the flux angle errors under method A and the proposed method when there is a leakage inductance mismatch. In the case of no-load condition, the proposed method almost has the same errors as method A. However, the proposed method shows much smaller errors when 50% or 100% rated load torque is applied, with steady-state errors kept within 0.05 rad.

Fig. 7 shows the flux angle error comparison results for stator resistance mismatch. As we can see, both schemes show small field orientation errors across the full load power range. Fig. 8(a)

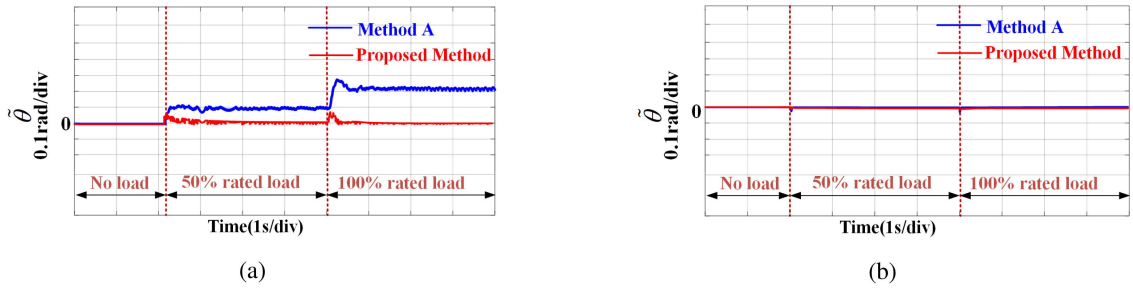

Fig. 8. Flux angle error comparison results for the different cases. (a) $\hat{R}_s = 0.5R_s$, $\hat{L}_\sigma = 0.5L_\sigma$. (b) $\hat{R}_s = R_s$, $\hat{L}_\sigma = L_\sigma$.

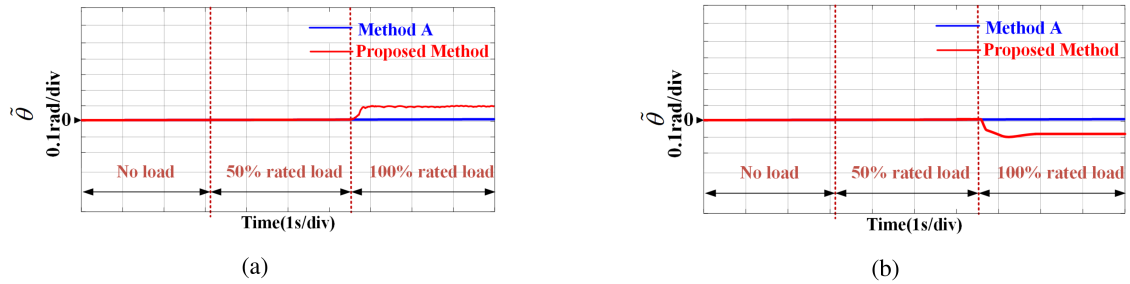

Fig. 9. Flux angle errors in the case of mutual inductance mismatch. (a) $\hat{L}_m = 0.5L_m$. (b) $\hat{L}_m = 1.5L_m$.

shows the flux angle error results in the case of stator resistance and leakage inductance mismatch. As seen, the errors under the proposed scheme are much smaller than those of method A when load is applied. Fig. 8(b) shows the results in the case of accurate stator resistance and leakage inductance. The errors under the proposed method are nearly equal to method A over the entire load power range.

The flux angle errors under 50% variation of mutual inductance are depicted in Fig. 9. As seen, method A is robust to mutual inductance mismatch across the full load range. In the proposed method, there is an angle error of 0.1 rad (5.73°) under 100% rated load.

Based on the aforementioned discussion, the proposed method shows high robustness to leakage inductance and stator resistance mismatch over the entire load power range, and exhibits a certain tolerance for mutual inductance mismatch, which is in good agreement with the theoretical analysis.

VI. Experimental Results

All the conditions of the experiment are identical to the simulation. The mutual inductance is measured offline [35], as shown in Fig. 10, and updated by linear interpolation. Since linear interpolation is simple to implement, a slight of computational burden is added. The IM is fed by a three-phase voltage source inverter using the space vector pulsewidth modulation. Fig. 11 shows the prototype IM drive system with a TI TMS320F28335 DSP. Because calculating the actual rotor flux is very difficult in experiments, the rotor flux estimated by the Gopinath model with well-identified parameters is defined as the actual flux [24], [25].

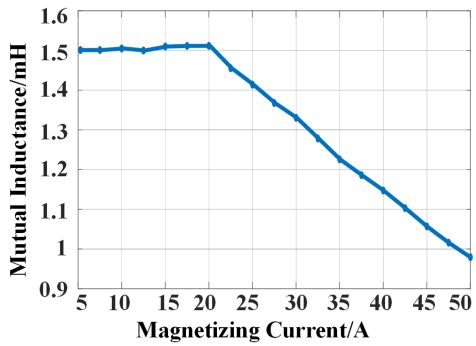

Fig. 10. Mutual inductance of the IM.

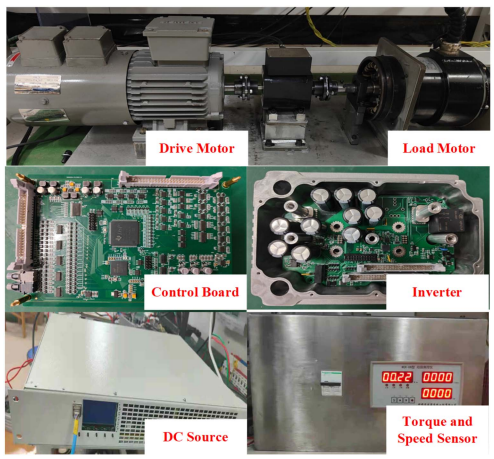

Fig. 11. Experimental platform.

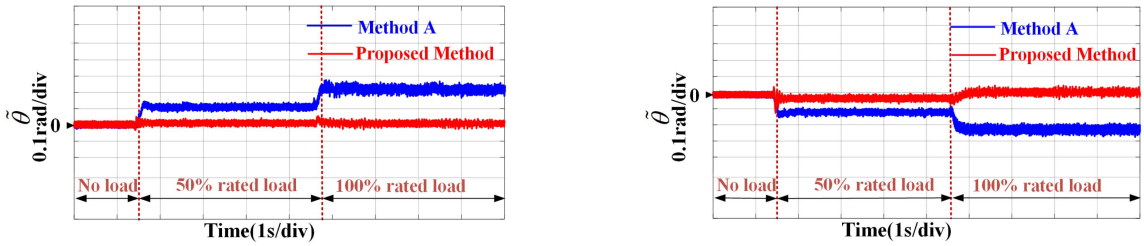

Fig. 12. Flux angle error results in the case of leakage inductance mismatch. (a) $\hat{L}_\sigma = 0.5L_\sigma$. (b) $\hat{L}_\sigma = 1.5L_\sigma$.

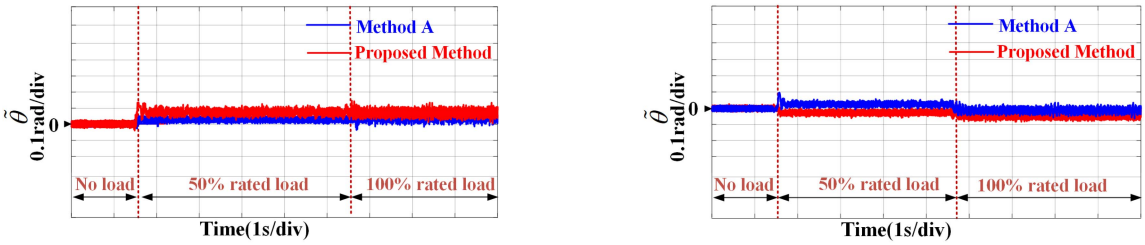

Fig. 13. Flux angle error results in the case of stator resistance mismatch. (a) $\hat{R}_s = 0.5R_s$. (b) $\hat{R}_s = 1.5R_s$.

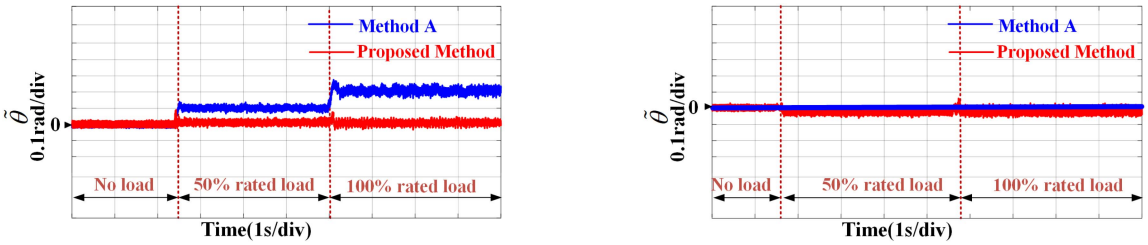

Fig. 14. Flux angle error results in the different cases: (a) $\hat{R}_s = 0.5R_s$, $\hat{L}_\sigma = 0.5L_\sigma$. (b) $\hat{R}_s = R_s$, $\hat{L}_\sigma = L_\sigma$.

A. *Flux Angle Error Comparisons*

Fig. 12 depicts the flux angle errors under method A and the proposed method when there is a leakage inductance mismatch. The variations of load power will significantly affect the field orientation accuracy under method A. However, the proposed method shows much higher field orientation accuracy despite the load power variations.

Fig. 13 shows the flux angle error comparison results with stator resistance detuning. Both methods show high robustness to stator resistance mismatch, with small flux angle errors over the entire load power range.

Fig. 14(a) demonstrates the flux angle errors in detuned cases of $\hat{R}_s = 0.5R_s$ and $\hat{L}_\sigma = 0.5L_\sigma$. It shows results similar to Fig. 12(a), the proposed scheme exhibits much smaller field orientation errors under load variations. Fig. 14(b) shows the flux angle errors in the case of accurate parameters. Both methods have nearly zero errors over the entire load power range.

Fig. 15 demonstrates the flux angle errors under 50% variation of mutual inductance. As seen, when a 100% rated load is applied, the angle errors under the proposed method are 0.1 rad, which is consistent with the simulation results.

B. *Speed Response Comparisons Under Load Variations*

The experimental results of speed response comparisons between the proposed method and method A are shown in Figs. 16–21. The speed command is 2000 r/min.

Fig. 16 shows the comparative results in the case of $\hat{L}_\sigma = 1.5L_\sigma$. When load torque changes, the speed convergence time under the proposed scheme is 0.14 s, which is smaller than 0.25 s with method A. From the waveforms of currents, the d-axis current under method A decreases to balance the change of rotor flux caused by the rise of the q-axis current. On the contrary, the d-axis current under the proposed scheme remains basically unchanged despite variations in load torque. From

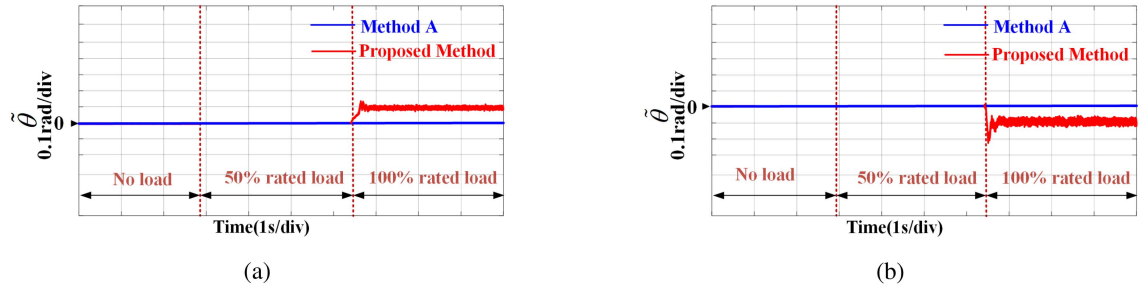

Fig. 15. Flux angle errors in the case of mutual inductance mismatch. (a) $\hat{L}_m = 0.5L_m$. (b) $\hat{L}_m = 1.5L_m$.

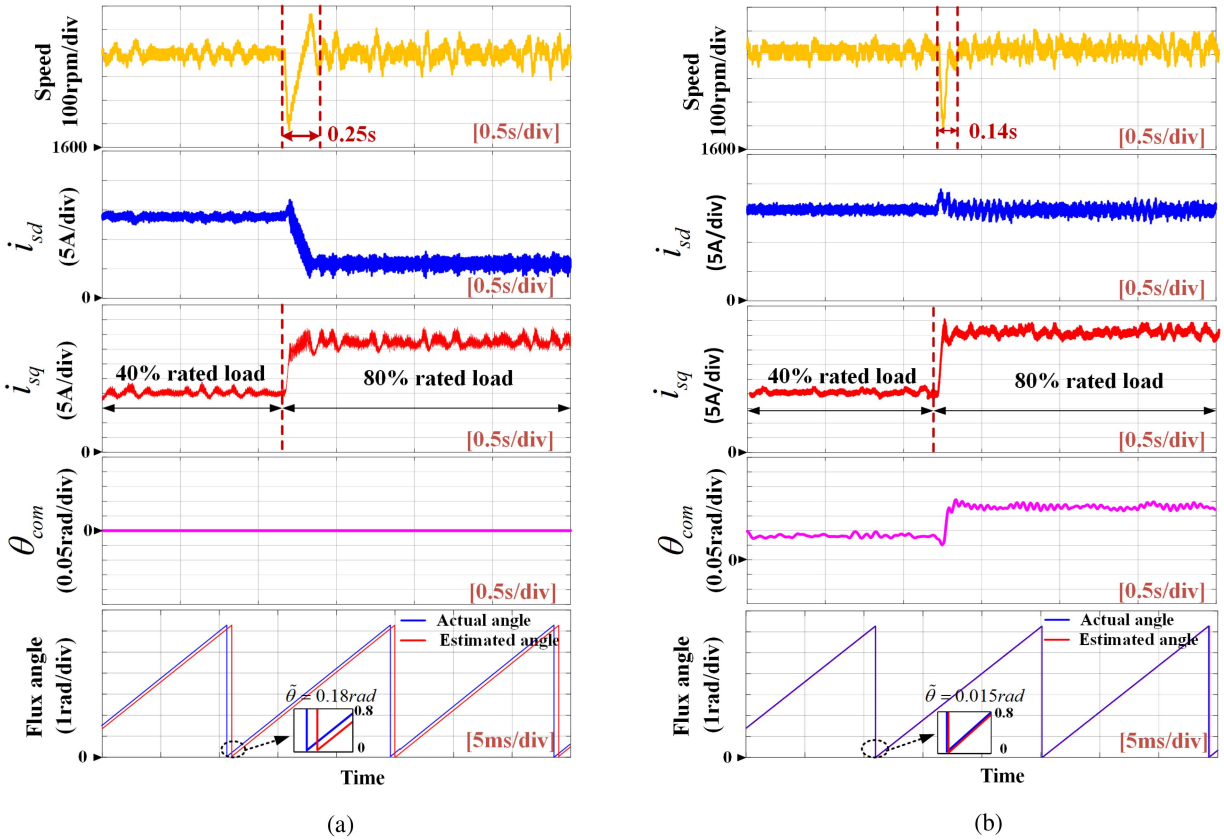

Fig. 16. Performance comparisons when load torque step change and $\hat{L}_\sigma = 1.5L_\sigma$. (a) Method A. (b) Proposed scheme.

the waveforms of flux angle, the compensation angle under the proposed scheme converges stably to 0.18 rad. And the estimated flux angle under the proposed scheme is more closely aligned with the actual one.

Fig. 17 shows the comparative results in the case of $\hat{L}_\sigma = 0.5L_\sigma$. Although the experiments are performed based on the same external conditions, significant differences can be found. First, the speed convergence time under the proposed scheme is 0.18 s, which is smaller than 0.26 s with method A. Second, it can be found that the d-axis current under the proposed scheme is almost constant, while the d-axis current under Method A varies with the change of working condition. Meanwhile, q-axis currents under different control schemes are also different. Obvious oscillations during the load change can be found on q-axis currents when method A is used. At last, different flux angle errors can be seen. The flux angle error under method A is 0.178 rad, and the error under the proposed one is only 0.035 rad. In fact, the different flux angle errors are the reason for the significant differences in speed response and d-axis and q-axis currents. It is well known that if flux angle errors are small, the rotor flux is mainly influenced by the d-axis current. However, if flux angle errors are large, the rotor flux is influenced by both d- and q-axes currents. In this case, the d-axis current varies with the change of the q-axis current to keep a constant rotor flux. As a result, the control performance of the IM is degraded.

Fig. 18 shows the comparative results in the case of $\hat{L}_\sigma = 0.5L_\sigma$ and $\hat{R}_s = 0.5R_s$. Because stator resistance mismatch

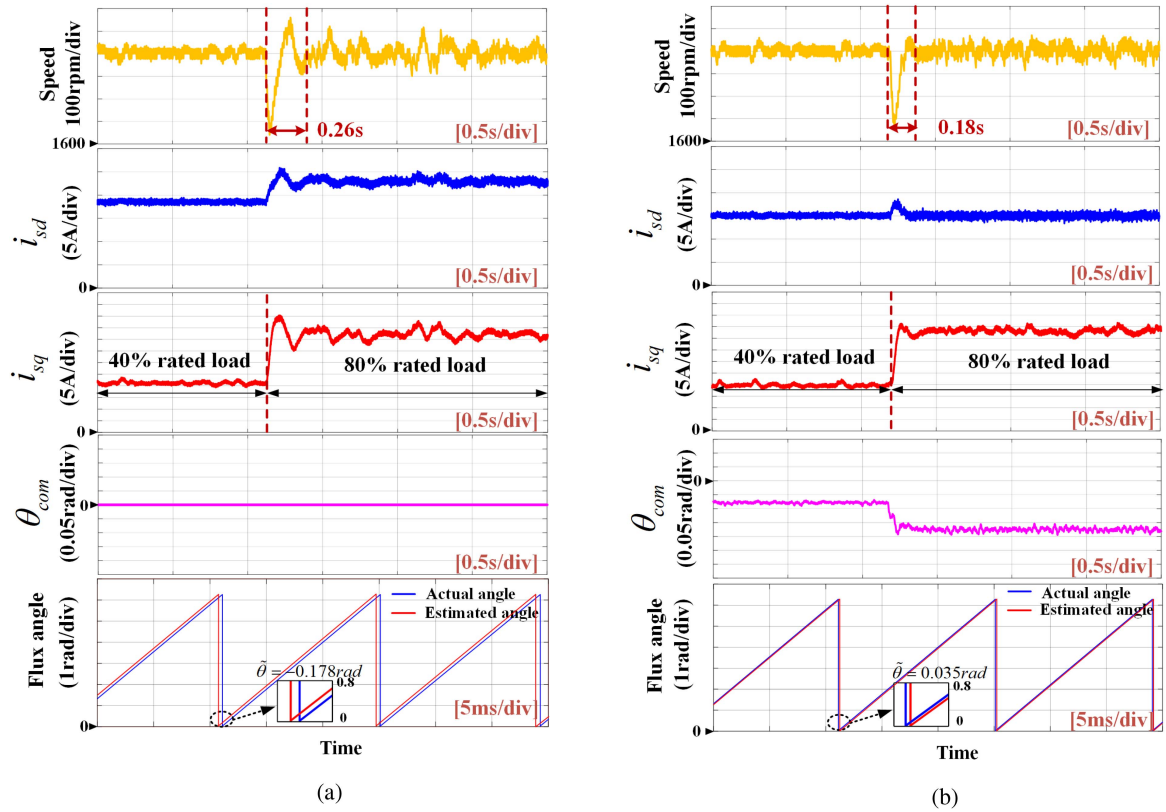

Fig. 17. Performance comparisons when load torque step change and $\hat{L}_\sigma = 0.5L_\sigma$. (a) Method A. (b) Proposed scheme.

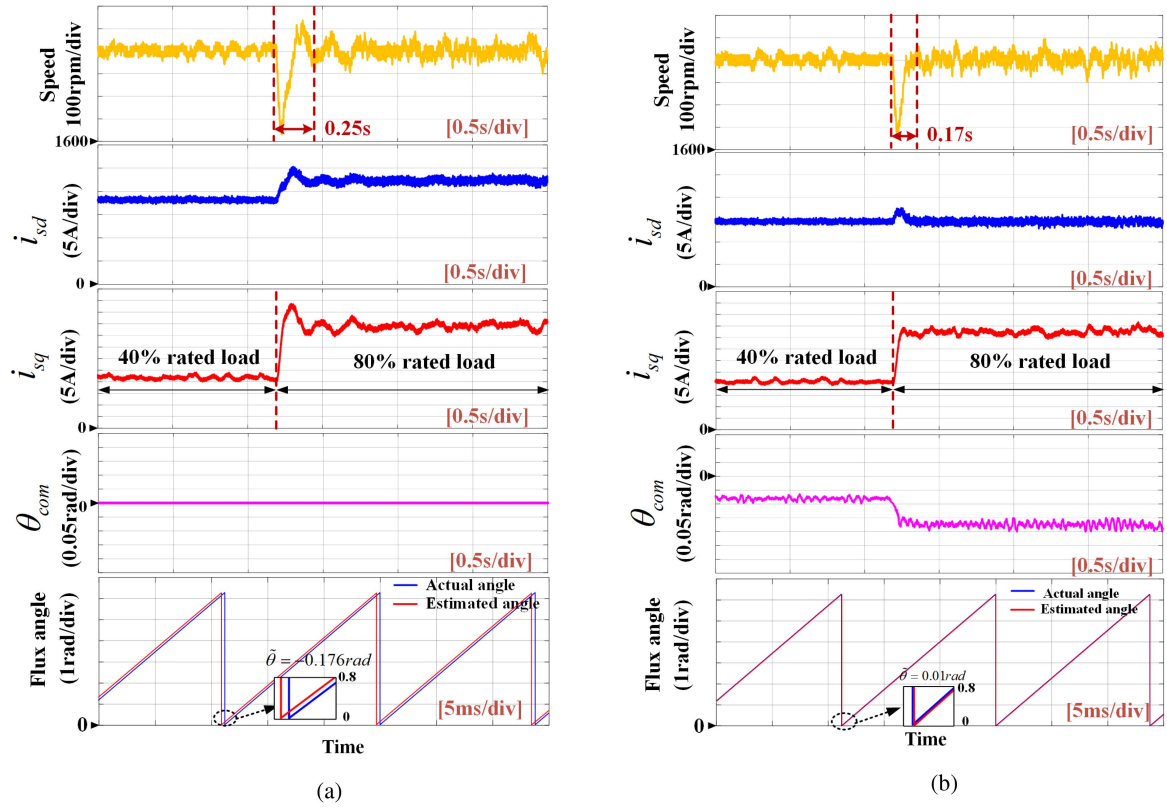

Fig. 18. Performance comparisons when load torque step change and $\hat{L}_\sigma = 0.5L_\sigma, \hat{R}_s = 0.5R_s$. (a) Method A. (b) Proposed scheme.

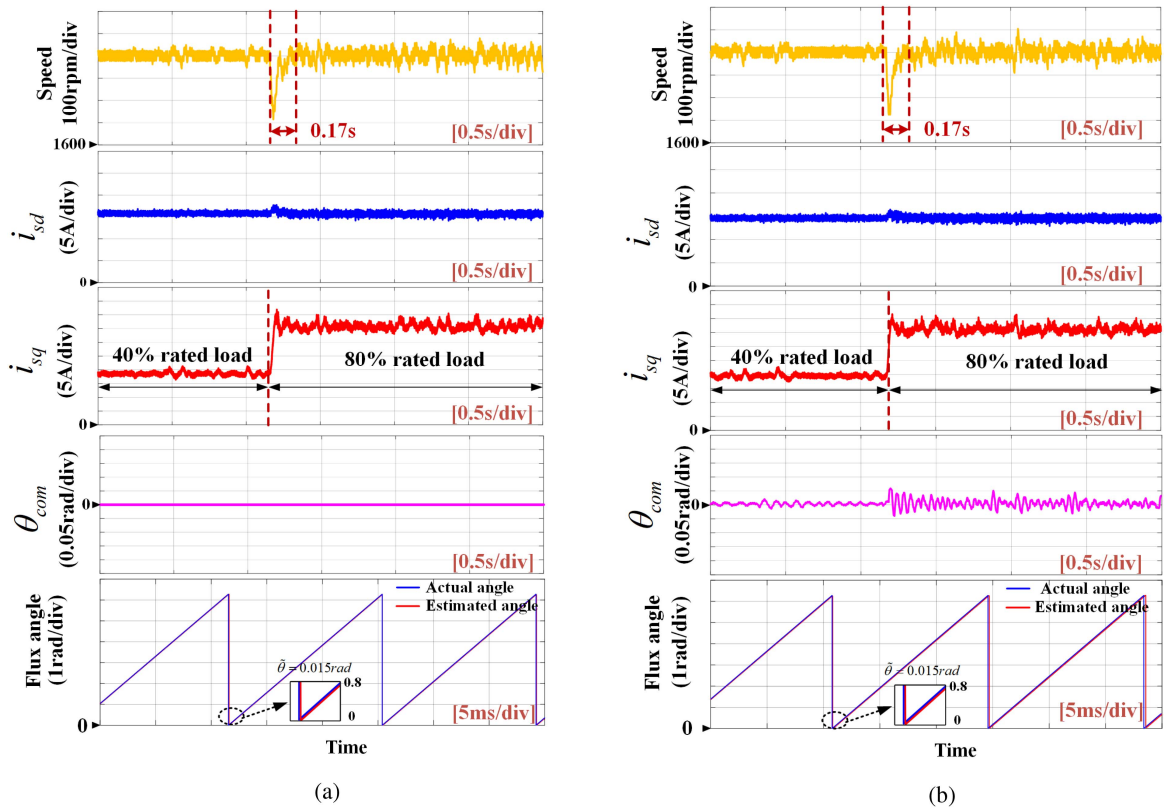

Fig. 19. Performance comparisons when load torque step change and $\hat{L}_\sigma = L_\sigma$, $\hat{R}_s = R_s$. (a) Method A. (b) Proposed scheme.

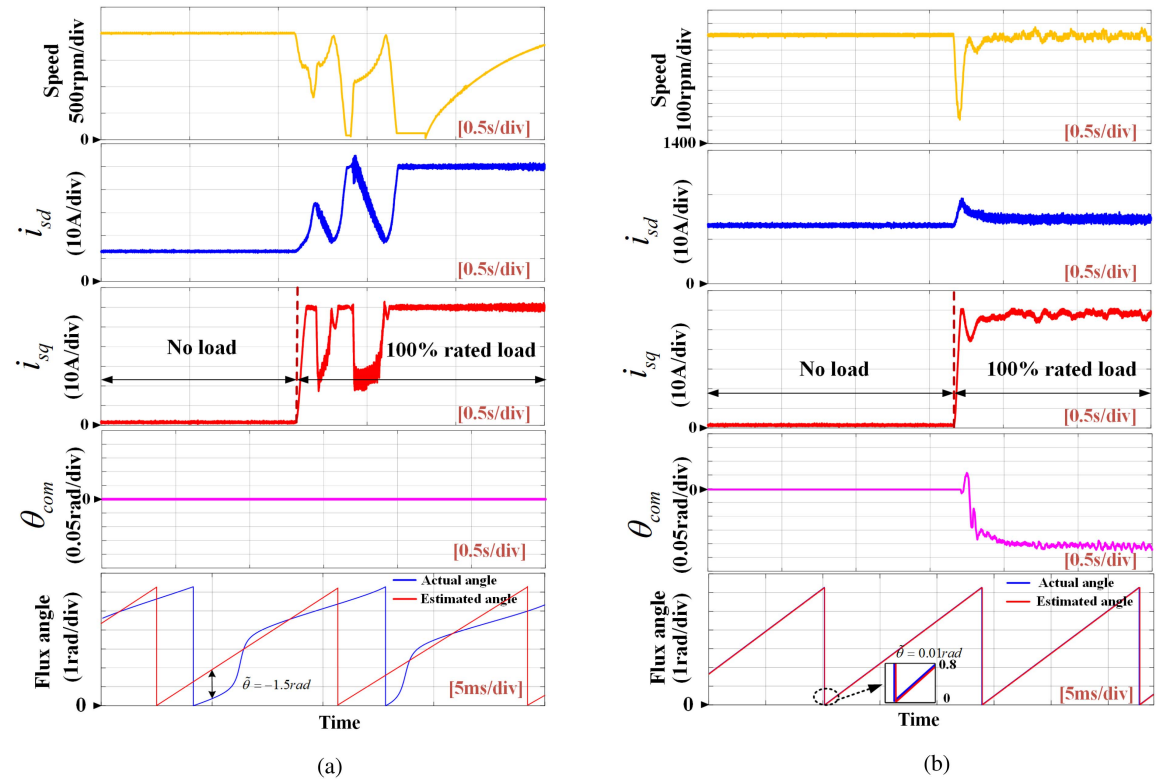

Fig. 20. Performance comparisons when load torque step change and $\hat{L}_\sigma = 0.5L_\sigma$. (a) Method A. (b) Proposed scheme.

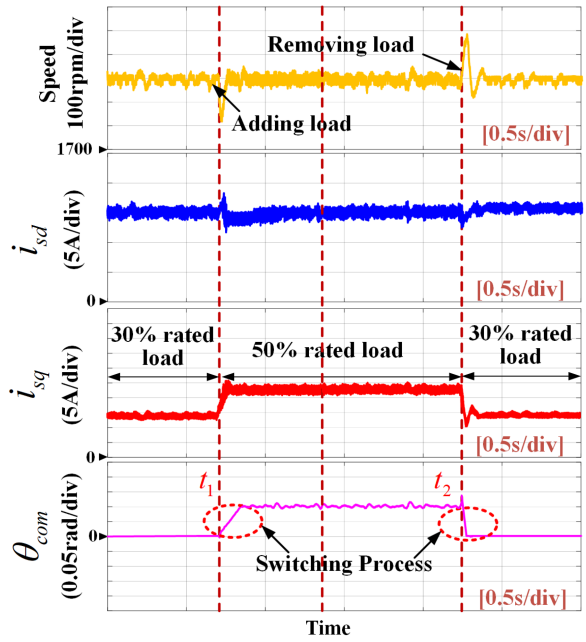

Fig. 21. Transient performance during algorithm switching.

has little effect on the flux angle errors under the two methods, the experimental results are essentially consistent with those in Fig. 17. The proposed scheme still shows much smaller field orientation errors and better speed drive performance.

Fig. 19 shows the comparative results in the case of accurate parameters. The proposed scheme exhibits almost the same performance as method A, because the compensation angle under the proposed scheme is nearly zero. This means that the proposed scheme is equivalent to method A under accurate parameter conditions.

Fig. 20 shows the comparative results in the case of $\hat{L}_\sigma = 0.5L_\sigma$. The load torque is increased from no-load to 100% of rated load torque. The RFO system based on method A is out of control, with current oscillations and field orientation failure. This is because when the leakage inductance is underestimated, a large value of k will cause the RFO system based on method A to lose its control. This issue is discussed in [30]. On the contrary, as depicted in Fig. 20(b), the proposed scheme improves the precision of field orientation and avoids the problem of being out of control.

The transient performance during algorithm switching is shown in Fig. 21. The load is added from 30% to 50% and back to 30% rated load torque. Method A enables under 30% rated load, and the field orientation method switches to method B when 50% rated load is applied. As seen, the switching method works well during the switching process.

The aforementioned results indicate that the proposed scheme shows high robustness against leakage inductance mismatch, leading to a better speed response of the system.

VII. Conclusion

In this article, a new field orientation scheme is proposed for RFO-based IM drives, which improves the robustness of voltage model-based IM drives against leakage inductance mismatch at high speed. The main advantage of the proposed field orientation method is that it combines the advantages of two methods. It not only preserves the high robustness of the method A for small $|k|$, but also the high robustness of method B for large $|k|$. Therefore, the influence of leakage inductance mismatch on the full load power range is reduced. The proposed scheme is compared with method A by simulation and experimental results. The proposed scheme shows high robustness against leakage inductance mismatch over the entire load power range. The flux orientation errors are reduced to less than 0.05 rad under full-load conditions. In addition, high-speed drive performance and antidisturbance ability of the system are improved under parametric uncertainties. Future research will be focused on improving the robustness of the Gopinath observer-based IM drives at low speed.

Appendix

$$f_1(k)=\tfrac{1}{2}+\sqrt{\tfrac{1}{4}-\left(1+\tfrac{1}{2}n\right)^2(\tilde{m}-k\tilde{n})^2+\left(1+\tfrac{1}{2}n\right)(\tilde{m}-k\tilde{n})\,k}. \tag{A.1}$$

$$f_2(k)=\left(1+\frac{\frac{1}{2}\tilde{n}-\frac{1}{2}n\tilde{L}}{1+\frac{1}{2}n}\right)\left(1-\tilde{L}\right)-\left(1+\tfrac{1}{2}n\right)(\tilde{m}k+\tilde{n}). \tag{A.2}$$

$$f_3(k)=\begin{cases}\left(\frac{1}{2}k-f_4(k)\right) & k>0\\ \left(\frac{1}{2}k+f_4(k)\right) & k<0.\end{cases} \tag{A.3}$$

$$f_4(k)=\sqrt{\tfrac{1}{4}k^2+f_2(k)-f_2^2(k)}. \tag{A.4}$$

$$k_m=-T_r\bar{\psi}_{rd}\frac{1+\frac{1}{2}\hat{n}+\frac{1}{2}\tilde{n}}{1+\frac{1}{2}n+\tilde{L}+\frac{1}{2}\tilde{n}}. \tag{A.5}$$

$$\omega_s=\frac{L_m i_{sq}-\bar{\psi}_{rq}}{T_r\bar{\psi}_{rd}}. \tag{A.6}$$

$$d=\frac{L_m\bar{i}_{sd}}{1+\frac{n}{2}-\frac{n}{2}\tilde{L}+\frac{\tilde{n}}{2}}\left(\left(-\tfrac{1}{2}+\left(1+\tfrac{n}{2}\right)^2\right)\tilde{n}+\left(1+\tfrac{n}{2}\right)^2k\tilde{m}-\tilde{L}\right). \tag{A.7}$$

References

[1] G. Pellegrino, A. Vagati, B. Boazzo, and P. Guglielmi, "Comparison of induction and PM synchronous motor drives for EV application including design examples," *IEEE Trans. Ind. Appl*, vol. 48, no. 6, pp. 2322–2332, Nov./Dec. 2012.

[2] G. B. Reddy, G. Poddar, and B. P. Muni, "Parameter estimation and online adaptation of rotor time constant for induction motor drive," *IEEE Trans. Ind. Appl.*, vol. 58, no. 2, pp. 1416–1428, Mar.-Apr. 2022.

[3] M. Bašić, D. Vukadinović, I. Grgić, and M. Bubalo, "Speed-sensorless vector control of an induction generator including stray load and iron losses and online parameter tuning," *IEEE Trans. Energy Convers.*, vol. 35, no. 2, pp. 724–732, Jun. 2020.

[4] I. Takahashi and T. Noguchi, "A new quick-response and high-efficiency control strategy of an induction motor," *IEEE Trans. Ind. Appl.*, vol. IA-22, no. 5, pp. 820–827, Sep. 1986.

[5] X. Xu and D. W. Novotny, "Implementation of direct stator flux orientation control on a versatile DSP based system," *IEEE Trans. Ind. Appl.*, vol. 27, no. 4, pp. 694–700, Jul./Aug. 1991.

[6] P. L. Jansen and R. D. Lorenz, "A physically insightful approach to the design and accuracy assessment of flux observers for field oriented induction machine drives," *IEEE Trans. Ind. Appl.*, vol. 30, no. 1, pp 101–110, Jan./Feb. 1994.
[7] S. Y. ang, P. Cao, and X. Zhang, "Stability analysis of q-axis rotor flux based model reference adaptive system updating rotor time constant in induction motor drives," *CES Trans. Elect. Mach. Syst.*, vol. 1, no. 2, pp. 109–116, Jun. 2017.
[8] X Y. u, M. W. Dunnigan, and B. W. Williams, "A novel rotor resistance identification method for an indirect rotor flux-orientated controlled induction machine system," *IEEE Trans. Power Electron.*, vol. 17, no. 3, pp. 353–364, May 2002.
[9] J. Kan, K. Zhang, and Z. Wang, "Indirect vector control with simplified rotor resistance adaptation for induction machines," *IET Power Electron.*, vol. 8, no. 7, pp. 1284–1294, 2015.
[10] A. Razzouk, A. Chériti, and P. Sicard, "Implementation of a DSP based real-time estimator of induction motors rotor time constant," *IEEE Trans. Power Electron.*, vol. 17, no. 4, pp. 534–542, Jul. 2002.
[11] P. Cao, X. Zhang, S. Yang, Z. Xie, and Y. Zhang, "Reactive-power-Based MRAS for online rotor time constant estimation in induction motor drives," *IEEE Trans. Power Electron.*, vol. 33, no. 12, pp. 10835–10845, Dec. 2018.
[12] E. Zerdali, "A comparative study on adaptive EKF observers for state and parameter estimation of induction motor," *IEEE Trans. Energy Convers.*, vol. 35, no. 3, pp. 1443–1452, Sep. 2020.
[13] S. Wade, M. W. Dunnigan, and B. W. Williams, "Comparison of stochastic and deterministic parameter identification algorithms for indirect vector control," in *Proc. IEE Colloq. Vector Control Direct Torque Control Induction Motors*, London, U.K., pp. 2/1–2/5, 1995.
[14] B. Regaya, A. Zaafouri, and A. Chaari, "Electric drive control with rotor resistance and rotor speed observers based on fuzzy logic," *Math. Problems Eng.*, vol. 2014, pp. 1–9, 2014.
[15] C. Ben Regaya, F. Farhani, A. Zaafouri, and A. Chaari, "A novel adaptive control method for induction motor based on backstepping approach using dSpace DS 1104 control board," *Mech. Syst. Signal Process.*, vol. 100, pp. 466–481, 2018.
[16] S. Munphal and S. Suwankawin, "A position-sensorless control of doubly fed induction machine by stator-equation-based adaptive reduced-order observer," *IEEE Trans. Power Electron*, vol. 37, no. 12, pp. 15186–15208, Dec. 2022.
[17] L. Harnefors and M. Hinkkanen, "Stabilization methods for sensorless induction motor drives—A survey," *IEEE J. Emerg. Sel. Topics Power Electron.*, vol. 2, no. 2, pp. 132–142, Jun. 2014.
[18] B. Robyns, F. Berthereau, G. Cossart, L. Chevalier, F. Labrique, and H. Buyse, "A methodology to determine gains of induction motor flux observers based on a theoretical parameter sensitivity analysis," *IEEE Trans. Power Electron.*, vol. 15, no. 6, pp. 983–995, Nov. 2000.
[19] A. Aliaskari, B. Zarei, S. A. Davari, F. Wang, and R. M. Kennel, "A modified closed-loop voltage model observer based on adaptive direct flux magnitude estimation in sensorless predictive direct voltage control of an induction motor," *IEEE Trans. Power Electron.*, vol. 35, no. 1, pp. 630–639, Jan. 2020.
[20] C. Luo, B. Wang, Y. Yu, C. Chen, Z. Huo, and D. Xu, "Decoupled stator resistance estimation for speed-sensorless induction motor drives considering speed and load torque variations," *IEEE Trans. Emerg. Sel. Topics Power Electron.*, vol. 8, no. 2, pp. 1193–1207, Jun. 2020.
[21] C. Lascu and G.-D. Andreescu, "Sliding-mode observer and improved integrator with dc-offset compensation for flux estimation in sensorless controlled induction motor," *IEEE Trans. Ind. Electron.*, vol. 53, no. 3, pp. 785–794, Jun. 2006.
[22] M. Comanescu, "Design and implementation of a highly robust sensorless sliding mode observer for the flux magnitude of the induction motor," *IEEE Trans. Energy Convers.*, vol. 31, no. 2, pp. 649–657, Jun. 2016.
[23] J. Kim, J. Ko, J. Lee, and Y. Lee, "Rotor flux and rotor resistance estimation using extended Luenberger-sliding mode observer (ELSMO) for three phase induction motor control," *Can. J. Elect. Comput. Eng.*, vol. 40, no. 3, pp. 181–188, 2017.
[24] J.-H. Kim, J.-W. Choi, and S.-K. Sul, "Novel rotor-flux observer using observer characteristic function in complex vector space for field-oriented induction motor drives," *IEEE Trans. Ind. Appl.*, vol. 38, no. 5, pp. 1334–1343, Sep./Oct. 2002.
[25] G. Jo and J. Choi, "Gopinath model-based voltage model flux observer design for field-oriented control of induction motor," *IEEE Trans. Power Electron*, vol. 34, no. 5, pp. 4581–4592, May 2019.
[26] P. L. Jansen, R. D. Lorenz, and D. W. Novotny, "Observer-based direct field orientation: Analysis and comparison of alternative methods," *IEEE Trans. Ind. Appl.*, vol. 30, no. 4, pp. 945–953, Jul./Aug. 1994.
[27] L. Harnefors and M. Hinkkanen, "Complete stability of reduced-order and full-order observers for sensorless IM drives," *IEEE Trans. Ind. Electron.*, vol. 55, no. 3, pp. 1319–1329, Mar. 2008.
[28] L. Harnefors, "Design and analysis of general rotor-flux-oriented vector control systems," *IEEE Trans. Ind. Electron.*, vol. 48, no. 2, pp. 383–390, Apr. 2001.
[29] M. Hinkkanen and J. Luomi, "Parameter sensitivity of full-order flux observers for induction motors," *IEEE Trans. Ind. Appl.*, vol. 39, no. 4, pp. 1127–1135, Jul./Aug. 2003.
[30] L. Harnefors, K. Pietiläinen, and L. Gertmar, "Torque-maximizing field-weakening control: Design, analysis, and parameter selection," *IEEE Trans. Ind. Electron.*, vol. 48, no. 1, pp. 161–168, Feb. 2001.
[31] S. -K. Sul, *Control of Electric Machine Drive System*. Piscataway, NJ, USA: IEEE Press, 2011.
[32] M. W. Degner, J. M. Guerrero, and F. Briz, "Slip-gain estimation in field-orientation-controlled induction machines using the system transient response," *IEEE Trans. Ind. Appl.*, vol. 42, no. 3, pp. 702–711, May/Jun. 2006.
[33] C. Attaianese, A. Damiano, G. Gatto, I. Marongiu, and A. Perfetto, "Induction motor drive parameters identification," *IEEE Trans. Power Electron*, vol. 13, no. 6, pp. 1112–1122, Nov. 1998.
[34] K. Wang, W. Yao, B. Chen, G. Shen, K. Lee, and Z. Lu, "Magnetizing curve identification for induction motors at standstill without assumption of analytical curve functions," *IEEE Trans. Ind. Electron.*, vol. 62, no. 4, pp. 2144–2155, Apr. 2015.
[35] M. S. Zaky, M. M. Khater, S. S. Shokralla, and H. A. Yasin, "Wide-speed-range estimation with online parameter identification schemes of sensorless induction motor drives," *IEEE Trans. Ind. Electron.*, vol. 56, no. 5, pp. 1699–1707, May 2009.
[36] L. Harnefors, S. E. Saarakkala, and M. Hinkkanen, "Speed control of electrical drives using classical control methods," *IEEE Trans. Ind. Appl.*, vol. 49, no. 2, pp. 889–898, Mar./Apr. 2013.
[37] A. Levant, "Exact differentiation of signals with unbounded higher derivatives," in *Proc. 45th IEEE Conf. Decis. Control*, San Diego, CA, USA, 2006, pp. 5585–5590.
[38] M. Fliess, C. Join, and H. Sira-Ramirez, "Non-linear estimation is easy," *Int. J. Model., Identification Control*, vol. 4, no. 1, pp. 12–27, 2008.
[39] R. Ortega, A. Astolfi, G. Bastin, and H. Rodriguez, "Stabilization of food-chain systems using a port-controlled Hamiltonian description," in *Proc. Amer. Control Conf.*, Chicago, IL, USA, 2000, pp. 2245–2249.

Peng Zeng (Student Member, IEEE) was born in Jiangxi, China, in 1996. He received the B.S. degree in electrical engineering and automatization in 2019 from Jiangsu University, Zhenjiang, China, and the master's degree in electrical engineering in 2022 from Central South University, Changsha, China, where he is currently working toward the Ph.D. degree in electrical engineering.

His research interests include power converter and motor control.

Yao Sun (Member, IEEE) was born in Hunan, China, in 1981. He received the B.S. and M.S. degrees in automation and the Ph.D. degree in control science and engineering from the School of Information Science and Engineering, Central South University, Changsha, China, in 2004, 2007, and 2010, respectively.

He is currently a Professor with the School of Automation, Central South University. His research interests include matrix converters, microgrids, and wind energy conversion systems.

Hanbing Dan (Senior Member, IEEE) was born in Hubei, China, in 1991. He received the B.S. degree in automation and the Ph.D. degree in control science and engineering from Central South University, Changsha, China, in 2012, and 2017, respectively.

He was a Visiting Researcher with the Faculty of Engineering, University of Nottingham, Nottingham, U. K., during 2017. Since 2018, he has been with the School of Automation, Central South University, where he is currently an Associate Professor. His research interests include power electronic and motor control.

Feng Zhou (Member, IEEE) received the B.Eng., M.Eng., and Ph.D. degrees in control science and engineering from Central South University, Changsha, China, in 2009, 2012, and 2017, respectively.

He is currently an Associate Professor with the School of Electronic Information and Electrical Engineering, Changsha University, Changsha. His main research interest includes high-performance predictive control technology for motor drive systems.

Mei Su (Member, IEEE) was born in Hunan, China, in 1967. She received the B.S. and M.S. degrees in automation and the Ph.D. degree in control theory and control engineering from the School of Information Science and Engineering, Central South University, Changsha, China, in 1989, 1992, and 2005, respectively.

She has been a Full Professor with the School of Automation, Central South University. Her research interests include matrix converter, adjustable speed drives, and wind energy conversion system.

Dr. Su is currently an Associate Editor for IEEE TRANSACTIONS ON POWER ELECTRONICS and IEEE TRANSACTIONS ON SUSTAINABLE ENERGY.

Patrick Wheeler (Fellow, IEEE) received the B.Eng. (Hons.) degree in electrical engineering and the Ph.D. degree in electrical engineering for his work on matrix converters from the University of Bristol, Bristol, U.K., in 1990 and 1994, respectively.

In 1993, he joined the Department of Electrical and Electronic Engineering, University of Nottingham, Nottingham, U.K., as a Research Assistant. In 1996, he joined the Power Electronics, Machines and Control Group, University of Nottingham, as a Lecturer. Since 2008, he has been a Full Professor with the Power Electronics, Machines and Control Group. He is currently the Head of the Power Electronics, Machines and Control Research Group, and the Global Director with the Institute of Aerospace Technology, University of Nottingham. He has authored and coauthored more than 750 academic publications in leading international conferences and journals.

Dr. Wheeler is a Member of the IEEE Power Electronics Society (PELs) Administrative Committee and is currently IEEE PELS Vice-President for Technical Operations.